

Constructing near-field and far-field with reactive metagratings: study on degrees of freedom

Vladislav Popov*

SONDRA, CentraleSupélec, Université Paris-Saclay, F-91190, Gif-sur-Yvette, France

Fabrice Boust†

SONDRA, CentraleSupélec, Université Paris-Saclay, F-91190, Gif-sur-Yvette, France and
DEMR, ONERA, Université Paris-Saclay, F-91123, Palaiseau, France

Shah Nawaz Burokur‡

LEME, UPL, Univ Paris Nanterre, F92410, Ville d'Avray, France

In this paper, we report that metamaterials-inspired one-dimensional gratings (or metagratings) can be used to control nonpropagating diffraction orders as well as propagating ones. By accurately engineering the near-field it becomes possible to satisfy power conservation conditions and achieve perfect control over all propagating diffraction orders with passive and lossless metagratings. We show that each propagating diffraction order requires two degrees of freedom represented by passive and lossless loaded thin “wires”. It provides a solution to the old problem of power management between diffraction orders created by a grating. The developed theory is verified by both 3D full-wave numerical simulations and experimental measurements, and can be readily applied to the design of wavefront manipulation devices over the entire electromagnetic spectrum as well as in different fields of physics.

I. INTRODUCTION

Back at the beginning of the 20th century, the problem of intensity distribution among different diffraction orders produced by a diffraction grating was one of the most important in optics [1]. Since then, a particular class of grating maximizing the intensity in a given diffraction order referred to as blazed gratings was studied in detail [1–4] and perfect blazing was demonstrated in nonspecular direction when only two orders propagate [5, 6]. In the context of antenna applications, highly efficient reflection and transmission at small diffraction angles was achieved by means of classical reflect- and transmit-arrays [7–9].

Amazing possibilities in manipulation of electromagnetic fields with engineered dense distributions of scatterers (metamaterials) have been demonstrated in the last two decades [10–13]. Extensive research in the area of metasurfaces, thin two-dimensional metamaterials, established a rigorous theoretical approach to arbitrary control reflection and refraction of an incident plane-wave [14–17]. In what follows we discuss examples of the perfect control (without spurious scattering) over the reflection/transmission that were demonstrated by means of a rigorous theory. Thus, perfect refraction in the first diffraction order and beam splitting in transmission with equal excitation of -1st and 1st diffraction orders by means of passive and lossless bianisotropic metasurfaces was presented in [18–20] and [21], respectively. In order to perform perfect nonspecular reflection with passive

and lossless metasurfaces, auxiliary surface waves have to be additionally excited [21–24]. Although it seems possible to design such metasurfaces the design procedure is still not well established [23, 24]. Huygens’ metasurfaces having equivalent electric and magnetic responses allow one to efficiently control diffraction from microwave [15] to optical frequencies [25] under the conditions of local normal power flow conservation and conjugate impedance matching [26].

In Ref. [27], *Radi et al.* have recently introduced the concept of metagratings which are an evolution of conventional one-dimensional (1D) diffraction gratings. The prefix “meta” implies that the grating is constructed from meta-atoms whose scattering properties can be judiciously engineered. Traditionally, in 1D gratings there is a profile modulation in one direction and a translational symmetry in the other. In metagratings, the translation invariant direction is engineered at a scale that is small compared to the wavelength such that it becomes possible to define an averaged macroscopic quantity like an impedance density [28]. The possibility to engineer the impedance density and an accurate analytical model allows one to overcome the limitations of metasurfaces. For instance, in Refs. [27–29] the authors, by means of theory and full-wave simulations, demonstrated the possibility of perfect nonspecular reflection and beam splitting in reflection with a metagrating composed of only a single unit cell per period. In order to realize perfect refraction in the 1st diffraction order three unit cells per period are required, as was shown analytically in [30]. Lately, experimental verification of perfect reflection in the -1st diffraction order has been reported by *Rabinovich et al.* in Ref. [31]. In Refs. [32, 33] the authors numerically and experimentally demonstrated efficient broad-

* uladzislau.papou@centralesupelec.fr

† fabrice.boust@onera.fr

‡ sburokur@parisnanterre.fr

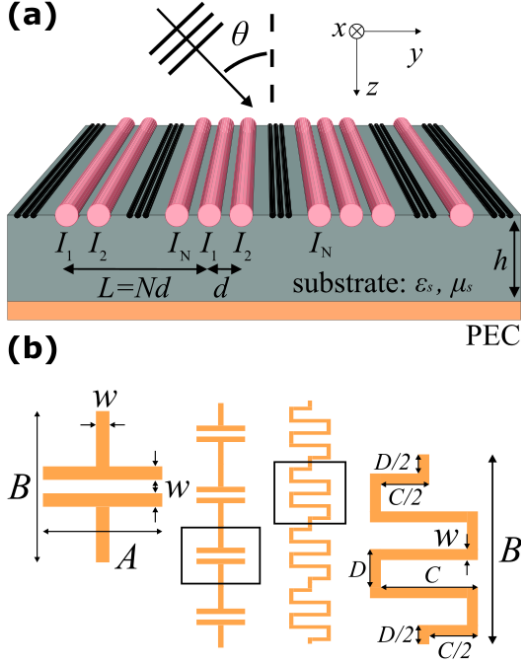


FIG. 1. Schematics of the considered physical system and elements of its practical implementation. (a) System under consideration: a periodic array of thin wires [large cylinders] placed on a PEC-backed dielectric substrate having relative permittivity ϵ_s , permeability μ_s and thickness h . The array is excited by a TE-polarized plane-wave incident at an angle θ . (b) Schematics of implementation at microwave frequencies of capacitively (left) and inductively (right) loaded PEC strips.

band nonspecular reflection with a 2-cell periodic structure capable of controlling two propagating diffraction orders.

The way towards control over arbitrary number of propagating diffraction orders by means of many unit cells based metagratings was outlined in Ref. [34] for a reflection configuration. Moreover, it was shown that when the number of degrees of freedom is equal to the number of propagating diffraction orders, perfect total control is possible only in the case when engineered active and lossy responses are available. Otherwise, there are scattering losses. In this paper, we report that metagratings can be used to control nonpropagating diffraction orders as well as propagating ones. By accurately engineering the near-field it becomes possible to satisfy power conservation conditions and achieve perfect control over all propagating diffraction orders with passive and lossless metagratings. In what follows, we study theoretically and validate experimentally the number of degrees of freedom required by each propagating diffraction order thus providing a solution to the old problem of power management between diffraction orders created by a grating.

II. PERFECT CONTROL OF DIFFRACTION:

TWO REACTIVE ELEMENTS PER AN ORDER

Theoretically, a metagrating is described as a one-dimensional periodic array of polarization line currents which are excited in thin loaded “wires” by a TE-polarized plane-wave incident at an angle θ and having the electric field along the wires. We consider a reflective-type metagrating when the wires are placed on top of a perfect electric conductor (PEC)-backed dielectric substrate. Schematics of the system under consideration is depicted in Fig. 1 (a). A grounded substrate should be carefully chosen in order to provide efficient excitation of line currents [i.e. $h \approx \lambda/(4\sqrt{\epsilon_s\mu_s - \sin^2(\theta)})$] and avoid excitation of waveguide modes [34].

Since the illuminated structure is periodic the wave reflected outside the substrate [$z < -h$] can be represented as a superposition of plane-waves $\sum_{m=-\infty}^{+\infty} A_m^{TE} e^{-j\xi_m y + j\beta_m z}$. The plane-waves have the tangential and normal components of wave vector equal to $\xi_m = k \sin[\theta] + 2\pi m/L$ and $\beta_m = \sqrt{k^2 - \xi_m^2}$, respectively, with k being the wavenumber outside the substrate. A simple model of metagratings allows one to find the amplitudes A_m^{TE} analytically (see details in Appendix A)

$$A_m^{TE} = -\frac{k\eta}{2L} \frac{(1 + R_m^{TE})e^{j\beta_m h}}{\beta_m} \sum_{q=1}^N I_q e^{j\xi_m(q-1)d} + \delta_{m0} R_0^{TE} e^{2j\beta_0 h} \quad (1)$$

where $\eta = \sqrt{\mu/\epsilon}$ is the characteristic impedance outside the substrate, δ_{m0} represents the reflection of the incident wave from the grounded substrate and R_m^{TE} is the Fresnel’s reflection coefficient. Equation (1) reveals that each of N line currents in a supercell contributes to the reflected plane-waves through the discrete Fourier transformation of the sequence I_q . Although there is an infinity of reflected plane-waves, only a finite number $M = r + l + 1$ of them is scattered in the far-field determining the diffraction pattern. r and l are the largest integers such that $\beta_r > 0$ and $\beta_{-l} > 0$. Currents I_q represent degrees of freedom that can be harnessed to control the amplitudes of the reflected fields as seen from equation (1).

Each polarization line current is excited in a thin wire characterized by its input-impedance Z_{in} and load-impedance Z_q densities. Necessary currents I_q can be obtained by loading wires with suitable load-impedance densities Z_q which are found from the following equation

$$Z_q I_q = E_q^{(exc)} - Z_{in} I_q - \sum_{p=1}^N Z_{qp}^{(m)} I_p. \quad (2)$$

The right-hand side of equation (2) represents the total electric field at the location of the q^{th} wire, $E_q^{(exc)}$ represents the excitation field (incident wave plus the wave reflected from the grounded substrate), $Z_{qp}^{(m)}$ are the mutual-impedance densities which account for the

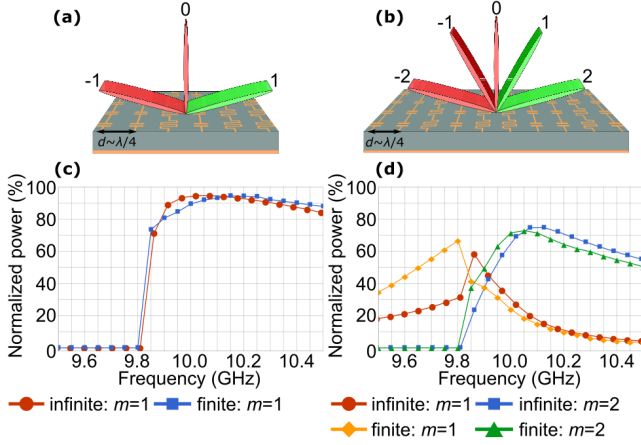


FIG. 2. Power management between propagating diffraction orders by the considered metagratings with six and eight unit cells per period: schematics (top row) and simulation data (bottom row). Result for infinite and finite size metagratings are presented. Figures in the top row depict excited (green lobes) and canceled (red lobes) propagating diffraction orders corresponding to the plots in the bottom row showing the 3D full-wave simulated frequency responses of the metagratings (i.e. part of total power scattered in a given diffraction order versus frequency). (a), (c) Example of nonspecular reflection at an angle of 80° by means of a metagrating with $N = 6$ unit cells per period. The finite size metagrating has 16 supercells. (b), (d) Example when out of five plane-waves reflected in the far-field, only the first (1/3 of total power) and second (2/3 of total power) propagating diffraction orders are excited with a metagrating having $N = 10$ unit cells in a period. The finite size metagrating has 8 supercells. In both examples, normal incidence is assumed.

interaction between the wires and between the wires and the grounded substrate. The details on the derivation of Eqs. (1) and (2) as well as the explicit expressions of the impedance densities can be found in Ref. [34]. For sake of the reader's convenience we place main parts of the derivations in Appendix A.

Total control of the diffraction pattern is possible by M line currents per supercell. However, we are particularly interested in purely reactive solutions of equation (2), since in practice it can be challenging to engineer active/lossy response of the load. Thus, the currents I_q should also satisfy the conditions of passivity and absence of loss

$$\Re \left[\left(E_q^{(exc)} - \sum_{p=1}^N Z_{qp}^{(m)} I_p \right) I_q^* \right] = \Re[Z_{in}] |I_q|^2, \quad (3)$$

where the asterisk symbol stands for the complex conjugate. Equation (3) represents a set of N quadratic algebraic equations with real and imaginary parts of currents being the variables and simply means that the q^{th} current radiates all the power spent on its excitation. Additional M (complex-valued) line currents are required to satisfy equation (3). Thus, $N = 2M$ line currents per supercell are necessary for establishing arbitrary diffraction pat-

terns exactly. Although there can be many line currents in a period, the distance between them is of the order of $\lambda/4$ (λ is the operating wavelength), which does not allow one to perform homogenization and introduce surface impedance.

From the physical point of view, the additional M currents are used to set the amplitudes A_m^{TE} of the surface waves (or nonpropagating diffraction orders, $m > r$ and $m < -l$) which would ensure equation (3). For a better understanding, let us consider an example of a perfect reflection in the 1st diffraction order of a plane-wave at normal incidence ($r = l = 1$). In this case, one has to cancel two propagating diffraction orders since there are three plane-waves reflected in the far-field and thus, the necessary number N of line currents per period is 6. First of all, one sets the amplitudes of the plane-waves in the far-field as $A_{-1}^{TE} = 0$, $A_0^{TE} = 0$ and $A_1^{TE} = e^{j\phi_1}$, where ϕ_1 is the phase of the anomalously reflected wave. Then the line currents I_q ($q = 1, 2, \dots, 6$) found from equation (1) ($m = -3, -2, \dots, 2$) are substituted into equation (3). The unknown (complex) amplitudes A_{-3}^{TE} , A_{-2}^{TE} and A_2^{TE} of the surface waves are found by solving equation (3), which automatically ensures the passive and lossless load-impedance densities Z_q calculated afterwards from equation (2).

III. DESIGN, SIMULATION AND EXPERIMENT

Once the necessary load-impedance densities are known, one has to come up with a practical implementation of the loads. In a general case, capacitive and inductive loads are required for such design implementation. As a proof of concept we demonstrate the design procedure for metagratings operating at microwave frequencies near 10 GHz. Thin metallic wires are realized as PEC strips having the input-impedance density $Z_{in} = k\eta H_0^{(2)}[kw/4]/4$ with $H_0^{(2)}$ being the Hankel function of the second kind and w being the width of strips. Capacitive and inductive responses can be achieved with the printed microstrip capacitors and inductors schematically shown in Fig. 1 (b). Load-impedance density Z_c of the printed capacitors can be approximately calculated by means of analytical formulas for the grid impedance of a PEC strips capacitive grid [35–37]

$$Z_c = -j\kappa_c \frac{\eta_{eff}}{2A\alpha}, \quad \alpha = \frac{k_{eff}B}{\pi} \ln \left[\frac{1}{\sin[\frac{\pi w}{2B}]} \right], \quad (4)$$

where A is the arms' length, $\eta_{eff} = \eta/\sqrt{\epsilon_{eff}}$, $k_{eff} = k\sqrt{\epsilon_{eff}}$, $\epsilon_{eff} = (1 + \epsilon_s)/2$, α is the grid parameter and B is the period along the x -direction. The formula (4) was already used in the context of metagratings in, e.g., [29] and [34]. Since PEC strips act intrinsically as inductors themselves ($\Im[Z_{in}] > 0$), the inductive load can be implemented by modulating the effective length of the strip through a meandering design process [37, 38]. Then, the

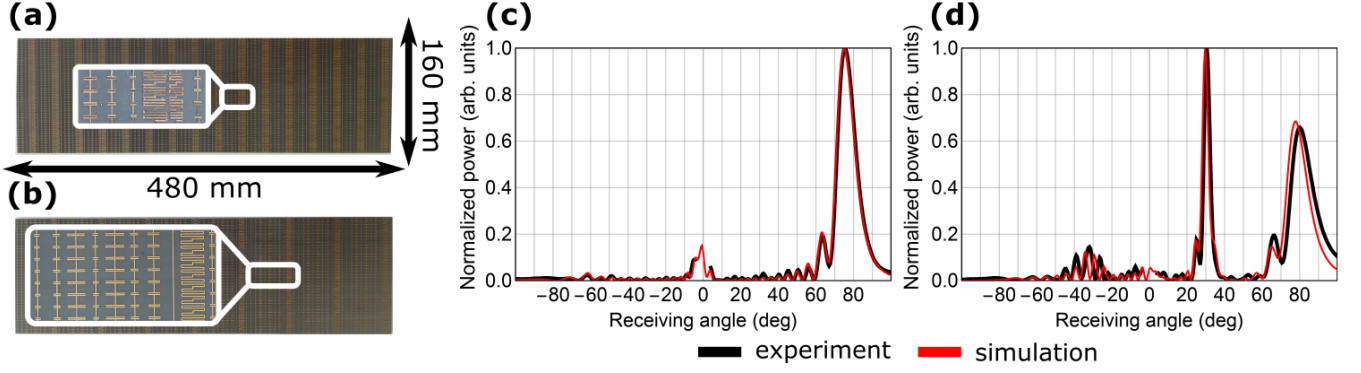


FIG. 3. Fabricated samples and comparison of the simulation and experimental data. (a), (b) Photographies of the samples performing (a) nonspecular reflection at 80 degrees ($N = 6$) and (b) splitting into two plane-waves propagating at 30 and 80 degrees ($N = 10$). (c), (d) Experimentally measured and numerically simulated scattering patterns: (c) nonspecular reflection at 10.1 GHz (main beam has 93% of total power), (d) unequal splitting into two plane-waves at 9.95 GHz (there are 31.5% of power in the 1st order and 63.5% in the second one).

inductive load-impedance Z_i density can be estimated as

$$Z_i = j \frac{1}{\kappa_i} \frac{l_{eff} \Im[Z_{in}]}{B}, \quad l_{eff} = C \left(\frac{B}{D} - 1 \right),$$

$$\Im[Z_{in}] \approx -\frac{k\eta}{2\pi} \left(\ln \left[\frac{kw}{8} \right] + \gamma \right), \quad (5)$$

where l_{eff} is the effective length of the meander, C and D are the parameters of the meander [see Fig. 1 (b)], and $\gamma \approx 0.5772$ is the Euler constant. Formula (5) is a rough approximation of the inductive load-impedance since it does not take into account the interaction between the meander strips and capacitive response on the incident wave. Geometrical parameters w , B and D are the same for all unit cells and fixed. Parameters A and C are found from Eqs. (4) and (5) for each unit cell accordingly to load-impedance densities calculated beforehand. The last step of the design procedure is to additionally adjust parameters A and C by performing a parametric sweep with respect to the scaling parameters κ_c and κ_i which are the same for different unit cells. In contrast to the design procedure of metasurfaces, here we perform simulations of a whole supercell having κ_c and κ_i as the only two free parameters. This allows one to account for interaction between unit cells and immediately arrive at the ultimate design. For a more detailed description of the design procedure see Appendix B.

The importance of the near-field control can be demonstrated by considering a simple example of a nonspecular reflection at extreme angles [21, 23, 24]. Namely, we consider the reflection of a normally incident plane-wave at the angle of 80 degrees. In this studied case, there are only three propagating diffraction orders (-1st, 0th and 1st), as shown by the schematics in Fig. 2 (a). Thus, for realizing the anomalous reflection one has to cancel scattering in the -1st and 0th diffraction orders, which requires six loaded wires per supercell implemented by passive and lossless elements. The second example we consider is the splitting of the normally incident plane-

wave into two reflected plane-waves propagating at 30 (first diffraction order) and 80 (second diffraction order) degrees. In contrast to commonly demonstrated examples of beam splitting, here the incident wave power is not equally distributed between the excited diffraction orders. Particularly, we design the sample to steer 1/3 of the total power in the first diffraction order and 2/3 in the second one. This scenario is schematically depicted in Fig. 2 (b) where there are five propagating diffraction orders controlled by ten loaded wires in a supercell. Other examples are also provided in Sec. IV.

The two metagratings are designed to operate at 10 GHz and tested in the following three steps. First, by means of 3D full-wave simulations we test the metagratings designs in an infinite array configuration by imposing periodic boundary conditions to a single supercell and by assuming plane-wave illumination. Figures 2 (c) and (d) demonstrate the frequency response of the infinite metagratings. It is seen that the efficiency is above 95% in both considered examples at the frequency of operation. The remaining 5% power is dissipated as heat in the substrate due to dielectric losses and as spurious scattering due to imperfections of the design. In a second step, 3D full-wave simulations are used to test finite size physical metagratings with a number of supercells corresponding to that used for fabrication of the experimental samples. In order to be able to further compare the results of these simulations to the experimental data, features of the experimental setup have to be taken into account. The fabricated samples have been tested in an anechoic chamber dedicated to radar cross section (RCS) bistatic measurements. Transmitting and receiving horn antennas are mounted on a common circular track of 5 m radius. A photo of the experimental setup is shown in Appendix. Physical sizes of the experimental samples are approximately 480 mm (y -direction) by 160 mm (x -direction), as illustrated in Figs. 3 (a) and (b). Thus the wavefront of the incident wave in the y -direction cannot be approximated by a plane-wave. To take this configu-

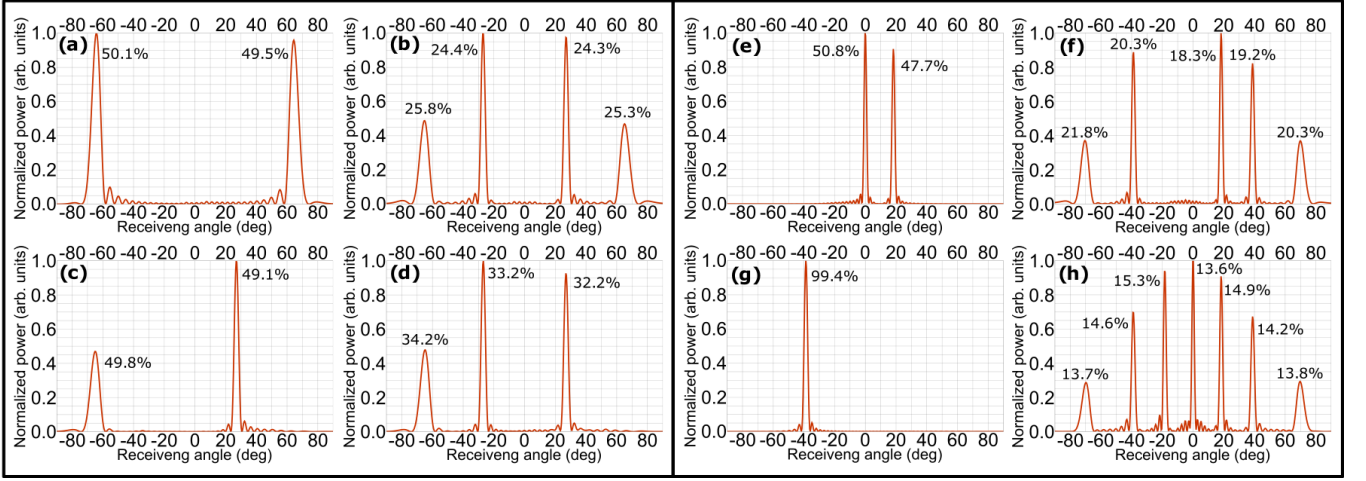


FIG. 4. Far-field scattering patterns from finite size metagratings under normally incident plane-wave obtained by means of 2D full-wave COMSOL simulations. Each finite size metagrating has 8 supercells. Numbers next to each lobe represent the part of power in a given lobe. All represented examples aim to demonstrate equal distribution of incident power between all excited propagating diffraction patterns (using equation (3) which assumes infinite samples). (a)–(d) Period $L = 2 \times 30/(\sin(65^\circ))$, there are five propagating diffraction orders. (a) -2^{nd} and 2^{nd} orders are excited. (b) -2^{nd} , -1^{st} , 1^{st} and 2^{nd} orders are excited. (c) -2^{nd} and 1^{st} orders are excited. (d) -2^{nd} , -1^{st} and 1^{st} orders are excited. (e)–(h) Period $L = 3 \times 30/(\sin(70^\circ))$, there are seven propagating diffraction orders. (e) 0^{th} and 1^{st} orders are excited. (f) All orders are excited apart from 0^{th} and -1^{st} . (g) only -2^{nd} order is excited. (h) All propagating orders are excited.

ration into account, simulations are performed assuming a cylindrical incident wave with periodic boundary conditions applied in the x -direction. The scattered fields are calculated on a circle enclosing the metagratings and are then extrapolated to a 5 m radius with the help of the Chu-Stratton formula [39, 40]. See Appendices C and D for details on the simulation data processing technique. Figures 2 (c) and (d) allow one to compare the efficiency of the finite size metagratings with the ideal case of the infinite metagratings. The discrepancy in Fig. 2 (d) at low frequencies stems from disappearance of the second orders what, clearly, has an impact on the performance of a finite size metagrating. However, this issue is to be studied yet. Finally, we compare the simulation results of the finite size metasurfaces with experimental data. In the current experiment, the transmitter is fixed and the receiver moves with 0.5 degrees step. The minimum angle value between the transmitter and the receiver for the scanning is 4 degrees. Under this experimental setup configuration, it is not possible to measure specular reflection in the experiment. Therefore, the performance of the fabricated samples can be estimated from the simulation data depicted in Figs. 2 (c) and (d). Figures 3 (c) and (d) compare the measured and simulated scattered patterns, where a good agreement can be observed.

IV. OTHER EXAMPLES BY 2D SIMULATIONS

So far we have demonstrate only two examples of metagratings for controlling diffraction patterns. However, the developed approach allows one to realize arbitrary

diffraction patterns. Figure 4 demonstrates different configurations of the far-field scattering pattern from metagratings of two different periods. The scattering pattern was obtained with 2D full-wave simulations performed by means of COMSOL Multiphysics as described in Appendix E. Metagratings in Fig. 4 were designed to equally split the power of normally incident plane-wave between excited propagating diffraction orders. Numbers next to each lobe represent the part of total power carried by a given beam. The imperfection are only due to the finite size of metagratings in the y -direction, i.e. finite number of periods. Indeed, the scattering problem for finite size objects is more complex than in case of infinite, truly periodic structures. Strictly speaking, the developed theory is valid for finite size metagratings only when an incident wave effectively illuminates a metagrating's area much greater than its period and much less than its whole size. For instance, it is the case for a Gaussian beam with the waist w_{GB} such that $1 \ll w_{GB}/L \ll N_s$ (N_s is the total number of supercells).

V. DISCUSSION AND CONCLUSION

The experimental validation results represent extreme examples in the control of diffraction patterns which are challenging or impossible to realize by other means. For instance, in order to perform large angle nonspecular reflection using a scalar reflective metasurface one has to significantly rely on numerical optimization techniques [23, 24]. Otherwise, one has to design a three layer scalar metasurface emulating omega-bianisotropic

load-impedance density (η/λ)	Z_1	Z_2	Z_3	Z_4	Z_5	Z_6	Z_7	Z_8	Z_9	Z_{10}
nonspecular reflection	$-j10.6$	$-j6.27$	$-j12.2$	$j12.5$	$j22.4$	$-j15.7$	—	—	—	—
beam splitting	$-j9.32$	$-j6.88$	$-j2.77$	$-j8.57$	$-j2.60$	$-j6.03$	$-j4.10$	$j0.38$	$j13.0$	$-j8.98$
geometrical parameters (mm)	A_1	A_2	A_3	C_4	C_5	A_6	—	—	—	—
nonspecular reflection	2.0	3.3	1.7	2.9	5.2	1.3	—	—	—	—
geometrical parameters (mm)	A_1	A_2	A_3	A_4	A_5	A_6	A_7	C_8	C_9	A_{10}
beam splitting	1.7	2.3	5.6	1.8	6.0	2.6	3.8	0	7.0	1.7

TABLE I. Parameters of metagratings presented in the main text. The indexes correspond to the numbered unit cells in Fig. 1.

response or a tensorial reflective metasurface [21, 22]. Up to date, neither the bianisotropic nor the tensorial metasurfaces have been validated experimentally or by means of 3D full-wave simulations for nonspecular reflection applications. On the other hand, metagratings presented in [34] and having the number of unit cells per supercell *equal* to the number of propagating diffraction orders would demonstrate maximum efficiency of only 70% in the shown examples.

To conclude, in this paper we demonstrate that to perfectly control the diffraction pattern each propagating diffraction order requires two degrees of freedom represented *only* by passive and lossless loaded thin wires. Thus, a metagrating having the number of unit cells per supercell twice the number of propagating diffraction orders allows one to set arbitrary complex amplitudes of all diffracted propagating plane-waves and accurately adjust the near-field in order to satisfy the conditions of passivity and absence of loss.

Although the proof of concept is done at microwave frequencies under the assumption of TE polarization, the main theoretical result is general. Significantly decreasing the number of unit cells per wavelength (comparing to metasurfaces) greatly relaxes the fabrication constraints what makes it easier to develop metagratings operating at the optical domain and capable of controlling all propagating diffraction orders. Recently, a metagrating performing perfect refraction in the first order at mid-infrared frequency range has been fabricated and experimentally tested [41]. Control over the reflection at infrared frequencies was demonstrated in Ref. [42] by means of numerical simulations. Meanwhile, presented formulas can be adapted for the case of TM polarization (and magnetic line currents) by means of duality relations [42, 43]. For example, a unit cell possessing magnetic response can be designed on the basis of a split ring resonator [27, 42]. Moreover, recent advances in the area of manipulating acoustic wavefronts [44–47] suggest that the developed theory can be also generalized for the needs of the acoustics community.

The possibility to develop metagratings operating at different frequency ranges as well as for other domains of physics such as acoustics opens an avenue for a plethora of applications. Particularly, metagratings can enrich the potential implementations of efficient flat optics components and tunable microwave antennas by achieving the

benefits of simple excitation, ease of fabrication and integration.

ACKNOWLEDGEMENTS

The authors acknowledge help of Anil Cheraly (ON-ERA) in conducting the experiment.

Appendix A: Theory

A single electric line current $\mathbf{J}(\mathbf{r}) = I\delta(y, z)\mathbf{x}_0$ radiates a cylindrical wave with the electric field in the form of Hankel function of the second time zeroth order $H_0^{(2)}[k\sqrt{y^2 + z^2}]$ (see Ref. [43])

$$E_x(y, z) = -\frac{k\eta}{4}IH_0^{(2)}[k\sqrt{y^2 + z^2}], \quad E_y = E_z = 0, \quad (\text{A1})$$

where $k = \omega\sqrt{\varepsilon\mu}$ and $\eta = \sqrt{\mu/\varepsilon}$. The electric field created by an infinite array of N equidistant line currents per period L is given by the following series

$$E_x(y, z) = -\frac{k\eta}{4} \sum_{q=1}^N \sum_{n=-\infty}^{\infty} I_q e^{-jk \sin[\theta]nL} \times H_0^{(2)}[k\sqrt{(y - nL - (q-1)d)^2 + z^2}], \quad (\text{A2})$$

the phase $\exp[-jk \sin[\theta]nL]$ appears because of the plane-wave illumination at angle θ . The Poisson's formula applied to the series of Hankel functions ($f(nL) = \exp[-jk \sin[\theta]nL]H_0^{(2)}[k\sqrt{(y - nL - (q-1)d)^2 + z^2}]$)

$$\sum_{n=-\infty}^{+\infty} f(nL) = \sum_{m=-\infty}^{+\infty} \int_{-\infty}^{+\infty} \frac{dw}{L} f(w) e^{-j\frac{2\pi m}{L}w}. \quad (\text{A3})$$

is used to express the series (A2) via plane-waves

$$E_x(y, z) = -\frac{k\eta}{2L} \sum_{q=1}^N \sum_{m=-\infty}^{\infty} \frac{I_q e^{j\xi_m(q-1)d}}{\beta_m} e^{-j\xi_m y - j\beta_m |z|}. \quad (\text{A4})$$

The Fourier transformation of Hanke function is given by the following formula

$$\int_{-\infty}^{+\infty} dw H_0^{(2)}[k\sqrt{(y-w)^2 + z^2}]e^{-j\xi_m w} = 2 \frac{e^{-j\xi_m y - j\beta_m |z|}}{\beta_m}. \quad (\text{A5})$$

The magnetic fields corresponding to Eqs. (A1) and (A4) can be found by means of the Maxwell equations. The effect of the grounded substrate on the field radiated by the array can be derived in the same manner as in Ref. [29]. After some algebra one would arrive at equation (1) for the complex amplitudes of propagating and nonpropagating diffraction orders outside the substrate. The factor R_m^{TE} appearing in the amplitudes corresponds to the Fresnel's reflection coefficient given by the following formula

$$R_m^{TE} = \frac{j\gamma_m^{TE} \tan[\beta_m^s h] - 1}{j\gamma_m^{TE} \tan[\beta_m^s h] + 1}, \quad \gamma_m^{TE} = \frac{k_s \eta_s \beta_m}{k \eta \beta_m^s}, \quad (\text{A6})$$

where $\beta_s = \sqrt{\varepsilon_s \mu_s k^2 - \xi_m^2}$, $\eta_s = \eta \sqrt{\mu_s / \varepsilon_s}$.

Mutual impedance densities $Z_{qp}^{(m)}$ take into consideration the interaction of the q^{th} wire (located in the zeroth period) with the substrate and adjacent wires and being expressed via the following formulas

$$\begin{aligned} Z_{qp}^{(m)} &= \frac{k\eta}{4} \sum_{n=-\infty}^{+\infty} H_0^{(2)}[k|(q-p)d - nL|] e^{-jk \sin[\theta] nL} \\ &+ \frac{k\eta}{2L} \sum_{m=-\infty}^{+\infty} e^{j\xi_m(p-q)d} \frac{R_m^{TE}}{\beta_m}, \quad q \neq p, \\ Z_{qq}^{(m)} &= \frac{k\eta}{2} \sum_{n=1}^{+\infty} \cos[k \sin[\theta] nL] H_0^{(2)}[knL] \\ &+ \frac{k\eta}{2L} \sum_{m=-\infty}^{+\infty} \frac{R_m^{TE}}{\beta_m}. \end{aligned} \quad (\text{A7})$$

The series containing R_m^{TE} correspond to the interaction with the substrate. The electric field at the location of the q^{th} wire in the zeroth period created by the rest of q^{th} wires and all other wires ($q \neq p$) is associated with the first terms constituting $Z_{qp}^{(m)}$ and $Z_{qq}^{(m)}$, respectively.

Appendix B: Design procedure and parameters of the experimental samples

The two metagratings presented as examples in the main text were designed to operate at 10 GHz ($\lambda \approx 30$ mm). In order to get the load-impedance densities, we start by setting the amplitudes of propagating diffraction orders. In the first case of nonspecular reflection of normally incident plane-wave at 80 degrees, period of the structure is $L_I = 30/\sin(80^\circ)$ mm and there are three propagating diffraction orders $A_{-1} = 0$, $A_0 = 0$ and $A_1 = 1/\sqrt{\cos(80^\circ)}$. It requires six polarization line currents per period separated by the distance $d_I = L_I/6$.

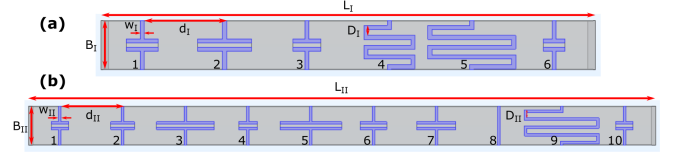


FIG. 5. Outline of the metagratings supercells geometry performing (a) nonspecular reflection at 80 degrees and (b) beam splitting in the first (1/3 of power) and second (2/3 of power) diffraction orders. Each unit cell of the metagratings is numbered in correspondence with Tab. I.

The complex amplitudes of three nonpropagating diffraction orders A_{-3} , A_{-2} and A_2 are found by numerically solving the system of equations (3). After all six amplitudes are known, we calculate the six polarization currents I_q from equation (1). Then, the load-impedance densities are found from equation (2). The same procedure is repeated for the other metagrating performing the splitting of normally incident plane-wave between the first (1/3 of power) and second (2/3 of power) propagating diffraction orders. Period of the metagrating is $L_{II} = 2 \times 30/\sin(80^\circ)$ mm and there are ten polarization line currents separated by the distance $d_{II} = L_{II}/10$. The complex amplitudes of the five propagating diffraction orders are set as $A_{-2} = 0$, $A_{-1} = 0$, $A_0 = 0$, $A_1 = \sqrt{1/3}/\sqrt{1 - (\lambda/L_{II})^2}$ and $A_2 = \sqrt{2/3}/\cos(80^\circ)$. Again, the complex amplitudes of nonpropagating diffraction orders A_{-5} , A_{-4} , A_{-3} , A_3 and A_4 are solutions of equation (3). Computed load-impedance densities can be found in Table I.

To design experimental samples parameters w , B and D are fixed and kept the same for all unit cells in a metagrating, as shown in Fig. 5. For the first sample performing nonspecular anomalous reflection, $w_I = 0.25$ mm, $B_I = 3$ mm and $D_I = 0.6$ mm. In the case of the second sample used for the beam splitting, these parameters are as follows: $w_{II} = 0.25$ mm, $B_{II} = 3.75$ mm and $D_{II} = 0.75$ mm. The used substrate is the F4BM220 with $\varepsilon_s = 2.2(1 - j10^{-3})$, $\mu_s = 1$, thickness of the substrate is $h = 5$ mm.

In order to find parameters A and C of each unit cell we use equations (4) and (5) presented in the main text and 3D full-wave simulations of a metagrating single supercell (as the ones in Fig. 5) with imposed periodic boundary conditions. We perform a parametric sweep with respect to the scaling parameters κ_c and κ_i until the model acts as desired. For the first and second samples the optimal parameters are $\kappa_c = 0.9$, $\kappa_i = 1.35$ and $\kappa_c = 0.92$, $\kappa_i = 2.66$, respectively. It is important to note that the scaling parameters are independent of the unit cell. In contrast to the design procedure of metasurfaces, here we perform simulations of a whole supercell having κ_c and κ_i as the only two free parameters. In this way we account for interaction between different unit cells and immediately arrive at the ultimate design. Geometrical parameters of the fabricated samples are specified in Table I.

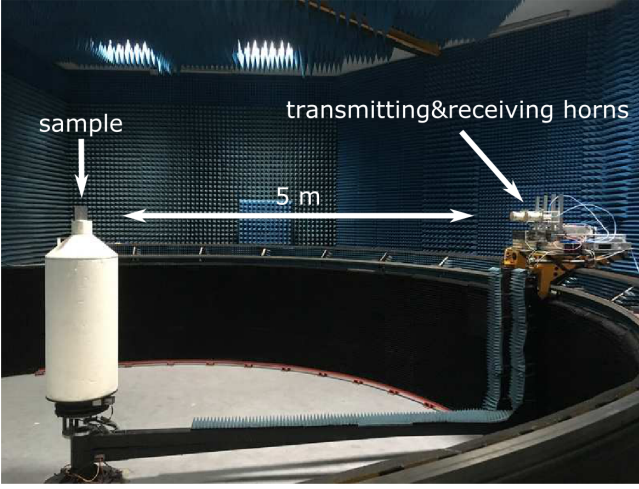


FIG. 6. Photography of the experimental setup used to measure the scattering patterns.

Appendix C: Processing of 3D simulation data

In the measurement setup (see, Fig. 6), the distance between the antennas and the sample is 5 m. This distance is not large enough to assume that the measurements are performed under the far-field condition. Indeed, the physical dimensions of the experimental samples are approximately 480 mm in the y -direction by 160 mm in the x -direction, see photographs in Figs. 3 (a) and (b). Thus the wavefront of the incident wave in the y -direction cannot be approximated by a plane-wave. To take it into account, simulations of the finite number of supercells (shown in Fig. 5) were performed assuming a cylindrical incident wave (phase center is 5 m away) with periodic boundary conditions applied in the x -direction. In order to correctly compare the simulation and measurement results, we harness the Chu-Stratton integration formula [39, 40] to extrapolate the field calculated on the circle C_1 of radius 258.7 mm (illustrated by the red curve in Fig. 7 (a)) enclosing the sample to the circle C_2 with 5 m radius

$$\mathbf{E}(y_2, z_2) = \frac{1}{4\pi} \oint_{C_1} (i\omega\mu[\mathbf{m} \times \mathbf{H}(y_1, z_1)] + [\mathbf{m} \times \mathbf{E}(y_1, z_1)] \times \nabla + [\mathbf{m}\mathbf{E}(y_1, z_1)]\nabla) G(y_2 - y_1, z_2 - z_1) dl. \quad (C1)$$

Here y_2 and z_2 are the coordinates of a point belonging to C_2 , the integrand contains the fields computed on C_1 , G is the free space green function and \mathbf{m} is the unit normal vector directed outward C_1 . As the simulations are performed with periodic boundary conditions in the x -direction, a 2D symmetry is assumed and, thus, we used $G(y, z) = jH_0^{(2)}[k\sqrt{y^2 + z^2}]/4$ as a Green function.

Fig. 7 (b) demonstrates the importance of the Chu-Stratton formula. It compares the scattering patterns from a metallic plate measured experimentally and obtained via numerical simulations under different conditions: (i) the metallic plate is under the normally incident

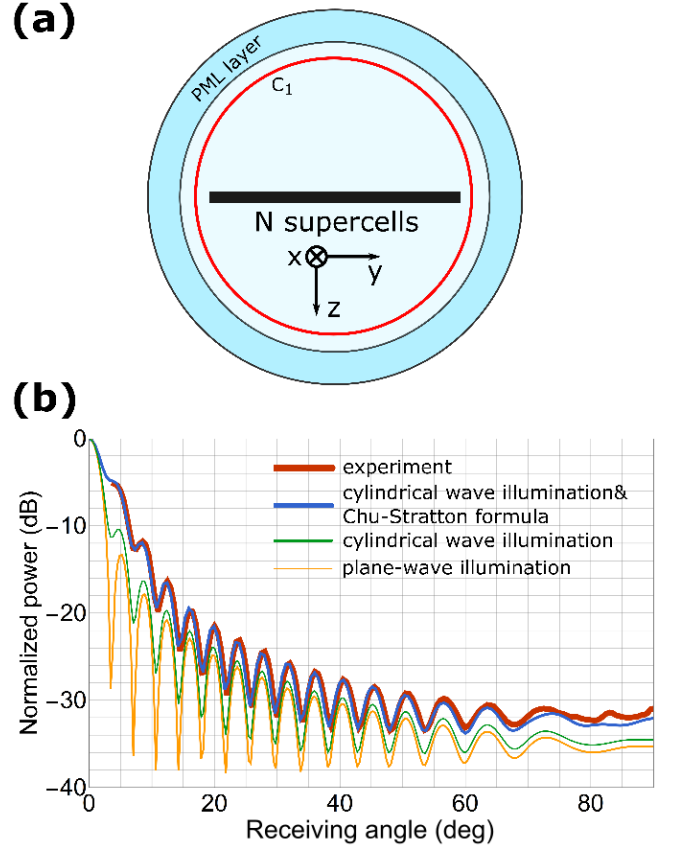


FIG. 7. (a) 2D cross section of the 3D full-wave simulation model of finite size metagrating. The red curve depicts the circle where the scattered fields were extracted. (b) Power scattering pattern from a metallic plate of length 485 mm simulated numerically under different conditions and compared to the experimental curve, frequency is 10 GHz.

plane-wave, far-field is calculated; (ii) the metallic plate is under the cylindrical wave illumination, phase center is at the distance 5 m, far-field is calculated; (ii) the metallic plate is under the cylindrical wave illumination, scattered field is processed by means of Chu-Stratton formula and pattern at the distance 5 m is built.

Appendix D: Calculation of the power scattered in given diffraction order

The diffraction pattern appeared when a plane-wave reflects from an infinite metagrating is represented by a finite number of plane-waves propagating at certain angles. The power scattered in the m^{th} propagating diffraction order is then calculated as $|A_m^{TE}|^2 \beta_m / \beta_0$ (assuming unit amplitude of the incident wave). However, when it comes to a finite size periodic structure under a plane-wave like illumination the pattern of the scattered field is much more complex. In this case we use the following formula to estimate the part of total power $\alpha_m(\nu)$

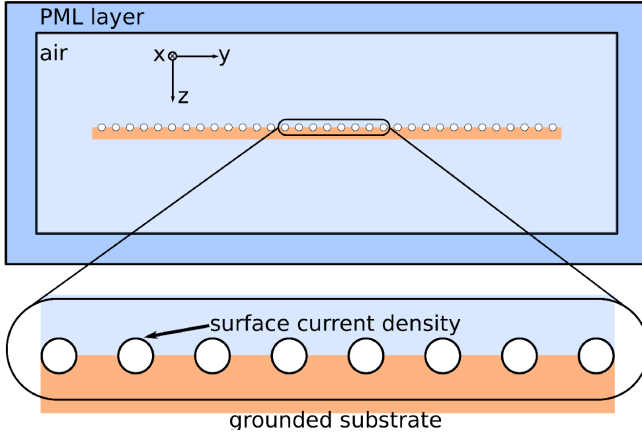


FIG. 8. Schematics of the 2D COMSOL model used for simulating metagratings. The white regions inside the circles are excluded from the model. Polarization line currents of effective radius r_0 (radius of the circles, it represents the input-impedance density) are simulated as surface current density: $\mathbf{J}_{es} = E_x/Z_q/(2\pi r_0)\mathbf{x}_0$ (\mathbf{x}_0 is the unit vector in the x direction). The total number of line currents (circles) is number of line currents per period times the number of periods.

scattered in a given diffraction order

$$\alpha_m(\nu) = \frac{\int_{\theta_1^m}^{\theta_2^m} P(\nu, \theta) d\theta}{\sum_{m=-l}^r \int_{\theta_1^m}^{\theta_2^m} P(\nu, \theta) d\theta}. \quad (\text{D1})$$

Here $P(\nu, \theta)$ represents the power scattered in the receiving angle θ , ν is the frequency. The integration is

performed only over the receiving angle range of half the maximum power of the beam corresponding to the m^{th} diffraction order. The summation in the denominator includes all propagating diffraction orders at the frequency ν . Angles θ_1^m and θ_2^m are found as follows. First, we accurately localize the maximum of the m^{th} diffraction order around the receiving angle $\sin^{-1}(\xi_m/k)$. Then, θ_1^m and θ_2^m correspond to the -3 dB of the power attenuation from the found maximum value.

Appendix E: 2D full-wave simulations of metagratings with COMSOL Multiphysics

A COMSOL model for 2D full-wave simulations of metagratings can be built in the following way. The principal element of a metagrating is a polarization line current which is modeled in COMSOL as surface current density assigned to the boundary of a circle, as shown in Fig. 8. The radius of the circle r_0 should be equal to the effective radius of a thin wire in order to get the correct value of the input-impedance density. It is important to exclude from the model the interior of the circles, otherwise one would get an incorrect value of the input-impedance density. The surface current density \mathbf{J}_{es} is set as follows: $E_x/Z_q/(2\pi r_0)\mathbf{x}_0$ (Z_q is the load-impedance density of the q^{th} thin wire). The array of circles is placed on a PEC-backed substrate (the circles' centers are on the top of the substrate) as shown in Fig. 8. In order to excite the model we use scattered field formulation and set a background field. The rest of the model is standard and can be understood from Fig. 8.

-
- [1] R.W. Wood, "The echelette grating for the infra-red," The London, Edinburgh, and Dublin Philosophical Magazine and Journal of Science **20**, 770–778 (1910), <https://doi.org/10.1080/14786441008636964>.
 - [2] Henry A. Rowland, "Gratings in theory and practice," The London, Edinburgh, and Dublin Philosophical Magazine and Journal of Science **35**, 397–419 (1893), <https://doi.org/10.1080/14786449308620425>.
 - [3] R. F. Stamm and J. J. Whalen, "Energy distribution of diffraction gratings as a function of groove form (calculations by an equation of henry a. rowland)," JOSA **36**, 2–12 (1946).
 - [4] M. Bredne, S. Johansson, L-E. Nilsson, and H. Åhlén, "Blazed holographic gratings," Optica Acta: International Journal of Optics **26**, 1427–1441 (1979), <https://doi.org/10.1080/713819919>.
 - [5] A. Hessel, J. Schmoys, and D. Y. Tseng, "Bragg-angle blazing of diffraction gratings*," J. Opt. Soc. Am. **65**, 380–384 (1975).
 - [6] M. Bredne and D. Maystre, "Perfect blaze in non-littrow mountings," Optica Acta: International Journal of Optics **28**, 1321–1327 (1981), <https://doi.org/10.1080/713820450>.
 - [7] D. M. Pozar, "Flat lens antenna concept using aperture coupled microstrip patches," Electronics Letters **32**, 2109–2111 (1996).
 - [8] J. Huang and J. A. Encinar, *Reflectarray antennas*, Vol. 30 (John Wiley & Sons, Hoboken, New Jersey, 2007).
 - [9] D. M. Pozar, "Wideband reflectarrays using artificial impedance surfaces," Electronics Letters **43**, 1–2 (2007).
 - [10] S. Jahani and Z. Jacob, "All-dielectric metamaterials," Nat. Nanotech. **11**, 23–36 (2016).
 - [11] S. B. Glybovski, S. A. Tretyakov, P. A. Belov, Y. S. Kivshar, and C. R. Simovski, "Metasurfaces: From microwaves to visible," Physics Reports **634**, 1–72 (2016).
 - [12] K. Sun, R. Fan, X. Zhang, Z. Zhang, Z. Shi, N. Wang, P. Xie, Z. Wang, G. Fan, H. Liu, C. Liu, T. Li, C. Yan, and Z. Guo, "An overview of metamaterials and their achievements in wireless power transfer," J. Mater. Chem. C **6**, 2925–2943 (2018).
 - [13] X.C. Tong, *Functional Metamaterials and Metadevices* (Cham, Springer, 2018).
 - [14] N. Yu, P. Genevet, M. A. Kats, F. Aieta, J.-P. Tetienne, F. Capasso, and Z. Gaburro, "Light propagation with phase discontinuities: Generalized laws of reflection and refraction," Science **334**, 333–337 (2011).

- [15] C. Pfeiffer and A. Grbic, “Metamaterial Huygens’ surfaces: Tailoring wave fronts with reflectionless sheets,” *Physical Review Letters* **110**, 1–5 (2013).
- [16] V. S. Asadchy, M. Albooyeh, S. N. Tsvetkova, A. Díaz-Rubio, Y. Ra’di, and S. A. Tretyakov, “Perfect control of reflection and refraction using spatially dispersive metasurfaces,” *Phys. Rev. B* **94**, 075142 (2016).
- [17] V. S. Asadchy, A. Díaz-Rubio, S. N. Tsvetkova, D.-H. Kwon, A. Elsakka, M. Albooyeh, and S. A. Tretyakov, “Flat engineered multichannel reflectors,” *Phys. Rev. X* **7**, 031046 (2017).
- [18] A. Epstein and G. V. Eleftheriades, “Arbitrary power-conserving field transformations with passive lossless omega-type bianisotropic metasurfaces,” *IEEE Transactions on Antennas and Propagation* **64**, 3880–3895 (2016).
- [19] M. Chen, E. Abdo-Sánchez, A. Epstein, and G. V. Eleftheriades, “Theory, design, and experimental verification of a reflectionless bianisotropic huygens’ metasurface for wide-angle refraction,” *Phys. Rev. B* **97**, 125433 (2018).
- [20] G. Lavigne, K. Achouri, V. S. Asadchy, S. A. Tretyakov, and C. Caloz, “Susceptibility derivation and experimental demonstration of refracting metasurfaces without spurious diffraction,” *IEEE Transactions on Antennas and Propagation* **66**, 1321–1330 (2018).
- [21] A. Epstein and G. V. Eleftheriades, “Synthesis of passive lossless metasurfaces using auxiliary fields for reflectionless beam splitting and perfect reflection,” *Phys. Rev. Lett.* **117**, 256103 (2016).
- [22] D.-H. Kwon and S. A. Tretyakov, “Perfect reflection control for impenetrable surfaces using surface waves of orthogonal polarization,” *Phys. Rev. B* **96**, 085438 (2017).
- [23] A. Díaz-Rubio, V. S. Asadchy, A. Elsakka, and S. A. Tretyakov, “From the generalized reflection law to the realization of perfect anomalous reflectors,” *Science Advances* **3** (2017), 10.1126/sciadv.1602714.
- [24] D. Kwon, “Lossless scalar metasurfaces for anomalous reflection based on efficient surface field optimization,” *IEEE Antennas and Wireless Propagation Letters* **17**, 1149–1152 (2018).
- [25] F. Monticone, N. M. Estakhri, and A. Alù, “Full control of nanoscale optical transmission with a composite metascreen,” *Phys. Rev. Lett.* **110**, 203903 (2013).
- [26] A. Epstein and G. V. Eleftheriades, “Floquet-Bloch analysis of refracting Huygens metasurfaces,” *Physical Review B - Condensed Matter and Materials Physics* **90**, 1–10 (2014).
- [27] Y. Ra’di, D. L. Sounas, and A. Alù, “Metagratings: Beyond the limits of graded metasurfaces for wave front control,” *Phys. Rev. Lett.* **119**, 067404 (2017).
- [28] A. Epstein and O. Rabinovich, “Unveiling the properties of metagratings via a detailed analytical model for synthesis and analysis,” *Phys. Rev. Applied* **8**, 054037 (2017).
- [29] O. Rabinovich and A. Epstein, “Analytical design of printed circuit board (pcb) metagratings for perfect anomalous reflection,” *IEEE Transactions on Antennas and Propagation* **66**, 4086–4095 (2018).
- [30] A. Epstein and O. Rabinovich, “Perfect anomalous refraction with metagratings,” *arXiv preprint arXiv:1804.02362* (2018).
- [31] O. Rabinovich, I. Kaplon, J. Reis, and A. Epstein, “Experimental demonstration and in-depth investigation of analytically designed anomalous reflection metagratings,” *arXiv preprint arXiv:1809.01938* (2018).
- [32] A. M. H. Wong and G. V. Eleftheriades, “Perfect anomalous reflection with a bipartite huygens’ metasurface,” *Phys. Rev. X* **8**, 011036 (2018).
- [33] A. M. H. Wong, P. Christian, and G. V. Eleftheriades, “Binary huygens metasurfaces: Experimental demonstration of simple and efficient near-grazing retroreflectors for te and tm polarizations,” *IEEE Transactions on Antennas and Propagation* **66**, 2892–2903 (2018).
- [34] V. Popov, F. Boust, and S. N. Burokur, “Controlling diffraction patterns with metagratings,” *Phys. Rev. Applied* **10**, 011002 (2018).
- [35] S. Tretyakov, *Analytical modeling in applied electromagnetics* (Artech House, 2003).
- [36] O. Luukkonen, C. Simovski, G. Granet, G. Goussetis, D. Lioubtchenko, A. V. Raisanen, and S. A. Tretyakov, “Simple and accurate analytical model of planar grids and high-impedance surfaces comprising metal strips or patches,” *IEEE Transactions on Antennas and Propagation* **56**, 1624–1632 (2008).
- [37] X. C. Wang, A. Díaz-Rubio, A. Sneek, A. Alastalo, T. Mäkelä, J. Ala-Laurinaho, J. F. Zheng, A. V. Räsänen, and S. A. Tretyakov, “Systematic design of printable metasurfaces: Validation through reverse-offset printed millimeter-wave absorbers,” *IEEE Transactions on Antennas and Propagation* **66**, 1340–1351 (2018).
- [38] X.-C. Wang, A. Díaz-Rubio, V. S. Asadchy, and S. A. Tretyakov, “Reciprocal angle-asymmetric absorbers: Concept and design,” *arXiv preprint arXiv:1801.09397* (2018).
- [39] J. A. Stratton and L. J. Chu, “Diffraction theory of electromagnetic waves,” *Phys. Rev.* **56**, 99–107 (1939).
- [40] J. A. Stratton, *Electromagnetic theory* (John Wiley & Sons, Hoboken, New Jersey, 2007).
- [41] Z. Fan, M. R. Shcherbakov, M. Allen, J. Allen, B. Wenner, and G. Shvets, “Perfect diffraction with multiresonant bianisotropic metagratings,” *ACS Photonics* **5**, 4303–4311 (2018).
- [42] V. Popov, M. Yakovleva, F. Boust, and S. N. Burokur, “Designing Metagratings Via Local Periodic Approximation: From Microwaves to Infrared,” *arXiv e-prints*, arXiv:1812.10164 (2018), arXiv:1812.10164 [physics.app-ph].
- [43] L. B. Felsen and N. Marcuvitz, *Radiation and scattering of waves*, Vol. 31 (John Wiley & Sons, 1994).
- [44] Y. Li, X. Jiang, R. Li, B. Liang, X. Zou, L. Yin, and J. Cheng, “Experimental realization of full control of reflected waves with subwavelength acoustic metasurfaces,” *Phys. Rev. Applied* **2**, 064002 (2014).
- [45] J. Li, C. Shen, A. Díaz-Rubio, S. A. Tretyakov, and S. A. Cummer, “Systematic design and experimental demonstration of bianisotropic metasurfaces for scattering-free manipulation of acoustic wavefronts,” *Nature communications* **9**, 1342 (2018).
- [46] D. Torrent, “Acoustic anomalous reflectors based on diffraction grating engineering,” *Phys. Rev. B* **98**, 060101 (2018).
- [47] P. Packo, A. N. Norris, and D. Torrent, “Inverse grating problem: Efficient design of anomalous flexural wave reflectors and refractors,” *Phys. Rev. Applied* **11**, 014023 (2019).